Applied Catalysis B: Environmental 244 (2019) 823–835

Contents lists available at ScienceDirect

Applied Catalysis B: Environmental

journal homepage: www.elsevier.com/locate/apcatb

Diphenamid degradation via sulfite activation under visible LED using Fe (III) impregnated N-doped TiO_2 photocatalyst

Amal Abdelhaleem[a], Wei Chu[a,*], Xiaoliang Liang[a,b]

[a] Department of Civil and Environmental Engineering, The Hong Kong Polytechnic University, Hung Hom, Kowloon, Hong Kong
[b] CAS Key Laboratory of Mineralogy and Metallogeny/Guangdong Provincial Key Laboratory of Mineral Physics and Materials, Guangzhou Institute of Geochemistry, Chinese Academy of Sciences, Guangzhou, 510640, China

ARTICLE INFO

Keywords:
Diphenamid
Visible LED
Sulfite activation
Impregnation
Fe-N doped TiO_2

ABSTRACT

Degradation of diphenamid (DPA) was examined by a novel process through sulfite activation by Fe impregnated N-doped TiO_2 (FeN-TiO_2) under visible LED (Vis LED). The FeN-TiO_2 was synthesized using an impregnation method and characterized by various techniques. The mechanism of sulfite activation by FeN-TiO_2 under Vis LED was proposed. The reaction mechanisms were further elucidated by investigating the XPS spectra of the catalysts before and after the reaction. Thirty intermediates were identified and twenty-four of them are newly reported. A new pathway was reported for the first time in the DPA studies through the rupture of benzene ring linkage. A higher mineralization degree was achieved using the FeN-TiO_2/sulfite/Vis LED process, which is not in accordance with previous reports on sulfite-based processes. The absence of sulfate adducts could provide a rational explanation of the higher mineralization degree during DPA degradation. Based on reusability test, the DPA degradation efficiency increased after successive usage of the catalyst. After the complete degradation of DPA, the leached Fe-ions were found to be negligible and sulfite was completely depleted. Considering several factors such as the cheap source of sulfite (an air pollutant waste from flue-gas desulfurization process), low cost of Fe, negligible leaching of Fe-ions, and high energy efficiency of Vis LED light, the FeN-TiO_2/sulfite/Vis LED process could be a practical and green technology for the removal of wastewater contaminants.

1. Introduction

Diphenamid (*N*, *N*-dimethyl-α-phenylbenzeneacetamide) (DPA), an acetanilide herbicide, has been widely applied for pre-emergence control of annual grasses and broadleaf weeds in ornamental plants [1,2]. Several studies on DPA have reported a relatively high water solubility (260 mg/L) and high environmental persistence [1]. DPA can persist for up to 10 months after its application to the soil [1,3,4]. Furthermore, DPA is nonvolatile and relatively stable under sunlight; thus its volatilization and photolysis are negligible [2]. Although DPA has a hazardous nature, its photocatalytic degradation and mineralization were reported to be inefficient [5]. Additionally, traditional UV light sources have been used in most of these studies, which require a high operational cost [5,6].

Recently, LED technology competes with traditional light sources due to its high energy efficiency, robustness, long lifetime, low cost, and environmental friendliness [7]. In our previous studies, a commercial visible LED lamp (Vis LED) was proven an efficient light source for herbicides' photodegradation [8,9], in which N-doped-TiO_2 photocatalyst (N-TiO_2) was confirmed to enhance visible light absorption substantially and generate active $^{\cdot}OH$ and $SO_4^{-\cdot}$ species via peroxymonosulfate (PMS) activation under Vis LED [8]. Although the N-TiO_2/PMS/Vis LED process exhibited a high performance for monuron decay, high dosages of PMS were needed to reduce the reaction time and to accomplish a high mineralization degree [8]. Besides, PMS can remain in the treated effluent after complete degradation of pollutants, which may impose unknown reactions in the environment [10,11].

Most recently, a novel approach by using sulfite as the radical source was proposed. Sulfite has been utilized in industry as a food or wine preservative or enhancer for preventing microbial spoilage [12]. Unlike the conventional radical sources, sulfite is a cheap, efficient, and eco-friendly chemical compared to persulfate (PS) and PMS [13], because it can be simultaneously degraded during the reaction along with the pollutants [10]. Furthermore, sulfite can be produced from flue-gas desulfurization process as a waste product, which renders it an attractive way by converting waste into valuable reactive radicals through a photocatalytic process [14].

Indeed, investigations on environmental applications of sulfite

* Corresponding author.
E-mail address: wei.chu@polyu.edu.hk (W. Chu).

https://doi.org/10.1016/j.apcatb.2018.11.085
Received 13 September 2018; Received in revised form 24 November 2018; Accepted 28 November 2018
Available online 06 December 2018

systems to replace PS or PMS are currently very limited. The generation of radicals from sulfite is primarily initiated by the formation of metal-sulfito complexes, which can be further decomposed to produce reactive radicals (Eqs. (1)–(6)) [10,15,16]. Some efforts have been devoted on sulfite activation using some transition metals such as copper (II) [17], nickel(II) [18], and Fe(II/III) [13,15,16,19,20]. Among these transition metals, Fe was considered as one of the most promising and economic candidates due to its abundance in the earth's crust, non-toxicity, durability, low cost, and high efficiency [21].

$$xSO_3^{2-} + M^{n+} \longrightarrow M(SO_3)_x^{n-2x} \longrightarrow xSO_3^{-\bullet} + M^{(n-1)+} \; (M = Fe,\ Cu,\ Co,\ Mn,\ etc.) \quad (1)$$

$$SO_3^{-\bullet} + O_2 \longrightarrow SO_5^{-\bullet} \quad (2)$$

$$SO_5^{-\bullet} + SO_5^{-\bullet} \longrightarrow 2SO_4^{-\bullet} + O_2 \quad (3)$$

$$SO_5^{-\bullet} + SO_3^{2-} \longrightarrow SO_4^{2-} + SO_4^{-\bullet} \quad (4)$$

$$SO_5^{-\bullet} + HSO_3^{-} \longrightarrow H^+ + SO_4^{2-} + SO_4^{-\bullet} \quad (5)$$

$$SO_4^{-\bullet} + H_2O \longrightarrow H^+ + SO_4^{2-} + {}^{\bullet}OH \quad (6)$$

In view of the above and to enhance N-TiO_2 as a visible light responsive photocatalyst for sulfite activation, the modification of N-TiO_2 with Fe ions (FeN-TiO_2) could be a reasonable combination. Some studies showed controversial results about the photoactivity after introducing transition metals. For instance, some investigations claimed that the presence of metal ions results in an enhancement in the photocatalytic activity of organic pollutants, while others stated that the addition of metal ions into TiO_2 has a detrimental effect [22–33]. However, it is believed that this approach has good potential to improve sulfite activation via the formation of metal-sulfito complexes as an additional radical source. N-TiO_2 was therefore modified with Fe ions using an impregnation method, which is a fast, low cost, and straightforward way without the need of complicated filtration steps [34]. Currently, limited attempts have been performed for sulfite activation using heterogenous catalysts such as $Zn_xCu_{1-x}Fe_2O_4$/sulfite and $CoFe_2O_4$/sulfite. However, no any information was provided about TOC reduction in the former [10] and a very poor TOC removal was observed in the latter [35]. Besides, $CoFe_2O_4$/sulfite system was found to be effective at alkaline media rather than neutral media [35]. Furthermore, conventional light sources have been utilized such as xenon lamps [10], which are energy consuming and require complicated cooling systems in real applications.

Based on the above analysis, a low-cost heterogeneous photocatalyst was synthesized through an impregnation technique for sulfite activation and its photocatalytic activity was evaluated for DPA degradation. To the best of our knowledge, no such comprehensive study was conducted for sulfite activation using the FeN-TiO_2/sulfite/Vis LED process and its environmental application on DPA decay.

2. Methodology

2.1. Chemicals and reagents

Diphenamid (DPA, 99.5%) was purchased from CHEM SERVICE, USA. Urea (≥99.5%), titanium isopropoxide (97%), HNO_3 (69%), isopropanol (99.8%), methanol (≥99.8%), tert-butanol (99.5%), sodium thiosulfate (≥95.5%), NaH_2PO_4 anhydrous (≥98.0%), Na_2SO_3 anhydrous (sodium sulfite, 98.0%), and absolute ethanol (100%) were supplied by SIGMA-ALDRICH. Fe $(NO_3)_3{\cdot}9H_2O$ (≥98.0%) was obtained from ALFA AEASAR. Acetonitrile (LC–MS grade) and formic acid (LC–MS grade) were obtained from TEDIA COMPANY, USA. For pH adjustment, HCl (37%) and NaOH (≥95.0%) were obtained from SIGMA-ALDRICH. All solutions and reagents were prepared using ultrapure water from Barnstead NANO water purification system (THERMO FISHER SCIENTIFIC INC., USA).

2.2. Catalyst synthesis

N-TiO_2 and undoped TiO_2 were synthesized by the sol-gel technique as described previously [8,9]. The modification of Fe^{III} ions onto N-TiO_2 was performed using an impregnation technique. Typically, 1 g of N-TiO_2 was added to 10 mL of ultrapure water, and the Fe $(NO_3)_3{\cdot}9H_2O$ was dissolved in the suspension. The suspension was then stirred for one hour, followed by drying at 80 °C overnight. The resulting powder was washed with sufficient amounts of ultrapure water and dried again at 80 °C overnight. After drying, the powder was thoroughly ground to obtain FeN-TiO_2 photocatalyst. The dosage of Fe-ions was controlled at 0.5 wt.%.

2.2. Characterization of catalysts

The catalysts were characterized by the X-ray diffraction (XRD), X-ray photoelectron spectroscopy (XPS), UV–vis spectroscopy techniques, Brunauer-Emmett-Teller specific surface area (BET SSA), transmission electron microscope (TEM), and energy dispersive X-ray spectrometry (EDX). The morphology was observed by transmission electron microscope (TEM, JEOL JEM-2100 F) operated at 200 kV. The element composition was characterized by an energy dispersive spectrometer attached to the TEM. The specific surface area (SSA) was calculated by a multipoint Brunauer-Emmett-Teller method on the basis of N_2 adsorption-desorption isotherms in the relative pressure (P/P_0) of 0.08–0.20. X-ray photoelectron spectroscopy (XPS) analyses were performed on a Thermo Scientific K-Alpha instrument equipped with an Al Kα source (10 mA, 14 kV) and operated at 1486.8 eV, and all binding energies were referenced to C 1s line at 284.8 eV. UV–vis diffuse reflectance spectra (UV–vis DRS) were recorded on PerkinElmer Lambda 950 UV–vis spectrometer equipped with an integrating sphere, in wavelength range of 200–800 nm at room temperature using $BaSO_4$ was used as the reflectance standard.

2.3. Photocatalytic degradation

Photocatalytic degradation of DPA was performed using two 100-W visible LED lamps (SUNSHINE Lighting Limited, Hong Kong) at a light intensity of 1540 lx (each) with a light spectrum (λ) from 420 to 700 nm. For the degradation tests, firstly, a predetermined amount of FeN-TiO_2 nanoparticles was dispersed into 100 ml of DPA solution and the suspension was stirred for 30 min in the dark to achieve the adsorption-desorption equilibrium. For all tests, the DPA decay after adsorption was nearly negligible and the concentration after adsorption was used as the initial concentration to guarantee an accurate comparison. Secondly, the photocatalytic reaction was initiated by adding the known concentration of sulfite. Generally, no pH adjustment was conducted for most experiments unless otherwise stated. The stock solution of sulfite was prepared freshly before each experiment, while the LED lamps were turned on for 30 min prior to irradiation to guarantee a stable light intensity. Once the photo-reaction started, 1 mL sample was withdrawn from the suspension at various time intervals, filtered by 0.45 μm syringe filter, quenched immediately by methanol, and then subjected to high-performance liquid chromatography (HPLC) measurements. For total organic carbon analysis (TOC), sodium thiosulfate was used instead of methanol for quenching radicals. During the entire test, the solution was continuously stirred and covered by a glass-petri dish to avoid evaporation. All experiments were conducted in replicates at laboratory temperature (23 ± 2 °C).

2.4. Analytical procedures

DPA concentration was quantified by HPLC, equipped with a Waters 515 pump, a Waters 2489 Dual absorbance detector, a Waters 717 plus autosampler, and a Restek C18 column (5 μm, 4.6 × 250 mm^2). The analysis was conducted using a mobile phase mixture of 50% acetonitrile and 50% deionized water, with a flow rate of 1 mL/min and at λ of

220 nm. The pH level was measured using a digital pH meter (HANNA instrument, HI 253). TOC measurements were performed using a Shimadzu TOC-L analyzer. DPA intermediates were examined by Ultraperformance Liquid Chromatography coupled with Electrospray Ionization Mass Spectrometry (UPLC-ESI-MS), and the detailed procedures are provided in Text S1 (Supporting Information). The sulfite concentration was analyzed by a colorimetric method using 5,5-Dithiobis-2-nitrobenzoic acid (DTNB) [10,20]. The concentrations of leached Fe ions were determined by atomic absorption spectroscopy (Agilent Technologies 200 Series AA).

3. Results and discussion

3.1. Characterization of catalyst

The XRD patterns of FeN-TiO_2 catalyst coincide with that of the undoped TiO_2 and N-TiO_2 in our previous study (data is not shown) [9]. Thus, the synthesized catalyst maintained a pure anatase phase, where the introduction of Fe ions did not influence the crystal phase of N-TiO_2 in a low-temperature impregnation process [36]. Additionally, no crystalline phase belonging to Fe compounds was observed in the XRD spectra, which may be ascribed to the low amount of Fe ions and/or the good dispersion of Fe ions on N-TiO_2 surface [32,36].

The morphological characteristics of different photocatalysts including N-TiO_2 (Fig. 1a) and FeN-TiO_2 (Fig. 1b) were investigated using HR-TEM analysis. For both N-TiO_2 and FeN-TiO_2, the particle size was ranging from 18 to 25 nm in diameter, without significant variation in the particle size after impregnating Fe ions on the N-TiO_2. No iron oxides were found around N-TiO_2 crystals, which further confirmed the existence of iron as ions [37].

Since the specific surface area (SSA) is a significant factor for enhancing the visible light photocatalytic activity, the BET SSA values were examined for both N-TiO_2 and FeN-TiO_2 as shown in Fig. 1c. As illustrated in Fig. 1c, the BET SSA of FeN-TiO_2 decreased slightly compared to that of N-TiO_2.

The surface atomic composition of N-TiO_2 and FeN-TiO_2 was semi-quantitatively analyzed by EDX (Fig. 1d). The nitrogen concentration was not detected due to the overlap of Ti, O, and nitrogen signals [38]. Nitrogen incorporation into TiO_2 lattice, however, was confirmed using XPS in our previous study [9]. The copper signal was shown in the N-TiO_2 and FeN-TiO_2 spectra owing to the use of the carbonated copper grid as a sample holder and the adventitious carbon was shown due to carbon contamination by CO_2 during the transfer of the samples. The copper and carbon signals were neglected for mass fraction calculations. Fortunately, Fe signal was detected in the FeN-TiO_2 (not in the N-TiO_2), and the iron atomic fraction was determined to be 0.42%. Additionally, the EDX mapping image of FeN-TiO_2 indicated a good dispersion of Fe on the N-TiO_2 surface and uniform distribution of particles (Fig. 1e).

As shown in the UV–vis diffuse reflectance spectra of FeN-TiO_2 (Fig. 1f), the band gap energy (E_g) of FeN-TiO_2 was 2.5 eV, obviously lower than that of N-TiO_2 (2.75 eV) [9], which may be attributed to the charge-transfer from the valence band of N-TiO_2 to Fe ions [39–41].

In order to investigate the surface composition of the synthesized catalyst, the FeN-TiO_2 catalyst was subjected to XPS analysis. As shown in Fig. 2.a, the full range survey of XPS spectrum revealed the presence of Ti (21.45 atomic %), O (43.4 atomic %), N (0.87 atomic %), Fe (1.43 atomic %), and C (32.85 atomic %) elements at binding energies of 458.63, 529.84, 399.69, 710.13, and 284.8 eV, respectively. Similar to EDX spectra, the adventitious carbon was shown in the XPS spectrum due to carbon contamination during the transfer of the samples to the XPS device. The Fe spectrum was shown in Fig. 2b to re-confirm the presence of Fe ions on the N-TiO_2 surface and to determine its oxidation state. As could be seen in Fig. 2b, two peaks corresponding to $Fe2p_{3/2}$ and $Fe2p_{1/2}$ were located at 710.13 and 722.58 eV, indicating the presence of Fe^{III} ions [39,41,42]. Since a low temperature (80 °C) was applied at the impregnation method, it is believed that the Fe ions existed mainly on the N-TiO_2 surface [36]. Based on the XPS analysis, it is suggested that the FeN-TiO_2 can be easily and efficiently synthesized via an impregnation technique.

According to XPS results, surface hydroxyl-groups density for both N-TiO_2 and FeN-TiO_2 photocatalysts was estimated using multiple Gaussian fitting and the results were shown in Fig. 2c and d, respectively. The asymmetric O 1 s peaks with two-band structure are observed, which can be deconvoluted into two contributions at 530.4 and 531.8 eV, which are contributed to the lattice oxygen (Ti-O) and surface hydroxyl groups (O—H), e.g., surface oxygen of hydroxyl species or adsorbed water species, respectively. The percentage of O—H on N—TiO_2 and FeN-TiO_2 was 13.3% and 14.3%, respectively (Table S1). This indicates that the impregnation of Fe ions on N-TiO_2 did not change the surface O—H density.

The point of zero charge of the FeN-TiO_2 catalyst was measured using batch equilibrium method and compared to that of the N-TiO_2 catalyst as determined previously [9]. As illustrated in Fig. S1 (Supporting Information), the pH_{PZC} of FeN-TiO_2 was determined to be 5.4, which is comparable to that of the N-TiO_2 (pH_{PZC} of 5.25 as estimated in our previous study).

3.2. Effect of various photocatalysts

The performance of undoped TiO_2, N-TiO_2, and FeN-TiO_2 was examined for DPA degradation under Vis LED and the results are shown in Fig. 3a. Apparently, undoped TiO_2 does not play a significant role in enhancing the photocatalytic activity under Vis LED within 360 min as expected due to its high band gap energy as reported in our previous study [9]. When using N-TiO_2 as a photocatalyst, a higher DPA decay was achieved (40%), suggesting the crucial role of N doping in enhancing the performance under Vis LED. After impregnating Fe ions on the N-TiO_2 surface, however, 36% degradation of DPA was achieved using the FeN-TiO_2, which is a little bit lower than that of the N-TiO_2. Comparable results were reported in previous studies after addition of transition metal ions on TiO_2 [23,24,43]. Although UV–vis diffuse reflectance spectra of FeN-TiO_2 exhibited an increased absorption in the visible range, there is no direct correlation between the visible light absorption and the photocatalytic activity [44]. The slightly higher activity of N-TiO_2 compared to that of FeN-TiO_2 may be justified by the larger BET SSA of N-TiO_2 compared to that of FeN-TiO_2, which results in more active sites on N-TiO_2.

3.3. Role of various processes

To verify the role of sulfite in the DPA decay different processes including sole Vis LED, sulfite/Vis LED, undoped TiO_2/sulfite/Vis LED, N-TiO_2/sulfite/Vis LED, and FeN-TiO_2/sulfite/Vis LED were further investigated, and the results are presented in Fig. 3b. It is apparent that the sole Vis LED process can barely cause any appreciable degradation of DPA; while the decay of DPA was insignificant by using sulfite/Vis LED (without a catalyst) and undoped TiO_2/sulfite/Vis LED. To investigate the contribution of Fe ions to the photocatalytic process, the DPA decay in the N-TiO_2/sulfite/Vis LED and FeN-TiO_2/sulfite/Vis LED processes was examined. Surprisingly, 80% DPA degradation in 12 min was observed by N-TiO_2/sulfite/Vis LED, implying that the sulfite can be activated using N doping without involvement of Fe. Compared to various heterogeneous and homogeneous activation processes of sulfite, it is worth mentioning that this is the first study to report the sulfite activation using non-metal doping. This observation can be rationalized by the activation of N-TiO_2 under Vis LED irradiation to produce $^{\cdot}OH$ and $SO_3^{-\cdot}$ according to Eqs. (7)–(13) [10]. Afterward, $SO_3^{-\cdot}$ can undergo subsequent reactions to give birth to $SO_4^{-\cdot}$ and $^{\cdot}OH$ as described in Eqs. (2)–(6) [10,15,16]. More interesting is that after impregnation of Fe ions, an obvious enhancement in the photocatalytic activity was observed (95%) due to the generation of additional $SO_3^{-\cdot}$ species

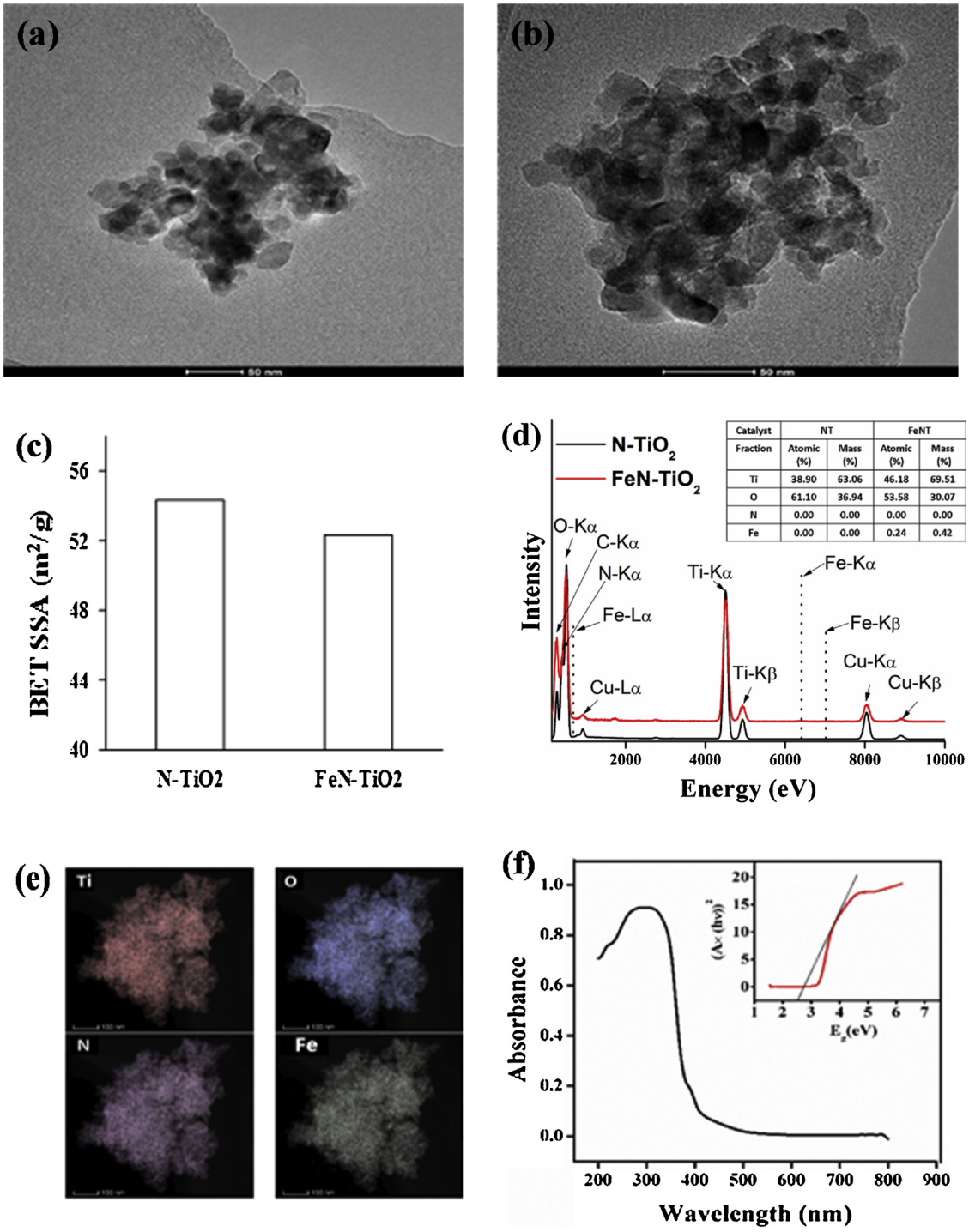

Fig. 1. Characterization of the synthesized catalysts. (a) HR-TEM of N-TiO_2. (b) HR-TEM of FeN-TiO_2. (c) BET SSA. (d) EDX spectrum of N-TiO_2 and FeN-TiO_2 catalysts. (e) EDX mapping image of the FeN-TiO_2. (f) UV–vis spectra of the FeN-TiO_2 catalyst.

through an additional pathway by forming metal-sulfito complex (Eqs. (14) and (15)) [10,15,20], which results in more $^{\cdot}OH$ and $SO_4^{-\cdot}$ (Eqs. (2)–(6)) in the solution [10,15,16]. The obtained results revealed the dual role of both N doping into TiO_2 lattice and Fe ions impregnation on the N-TiO_2 in sulfite activation, indicating that a synergistic effect was accomplished among FeN-TiO_2, sulfite, and Vis LED. Based on the above outstanding results, the FeN-TiO_2/sulfite/Vis LED process was therefore selected exclusively for the following tests.

$$FeN-TiO_2\ or\ N-TiO_2 + h\nu \longrightarrow FeN-TiO_2\ or\ N-TiO_2\ (e^- + h^+) \quad (7)$$

$$FeN-TiO_2\ or\ N-TiO_2(e^-) + O_2 \longrightarrow FeN-TiO_2\ or\ N-TiO_2 + {}^{\cdot}O_2^- \quad (8)$$

$${}^{\cdot}O_2^- + H^+ \longrightarrow HO_2^{\cdot} \quad (9)$$

$$2HO_2^{\cdot} \longrightarrow O_2 + H_2O_2 \quad (10)$$

$$H_2O_2 + {}^{\cdot}O_2^- \longrightarrow OH^- + {}^{\cdot}OH + O_2 \quad (11)$$

$$FeN-TiO_2\ or\ N-TiO_2(h^+) + HSO_3^- \longrightarrow FeN-TiO_2\ or\ N-TiO_2 + SO_3^{-\cdot} + H^+ \quad (12)$$

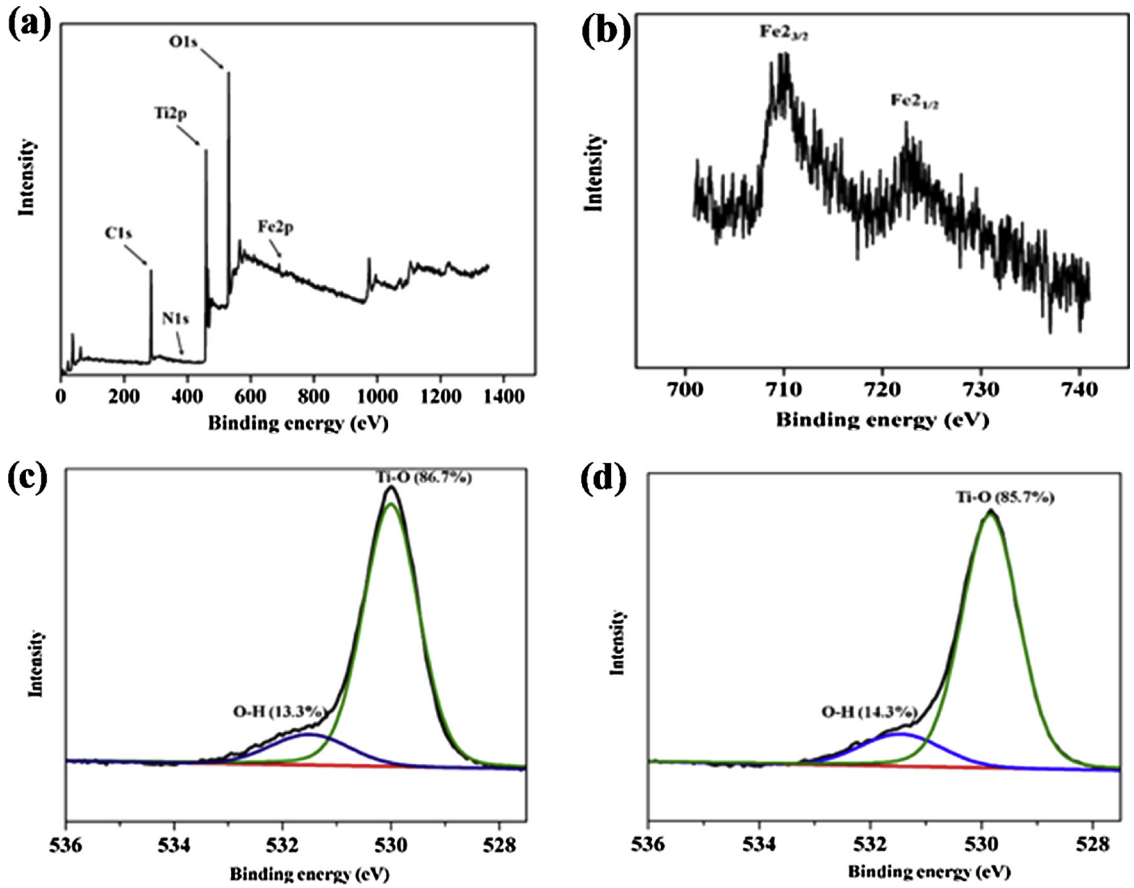

Fig. 2. (a) Full scan XPS spectra of the FeN-TiO_2 catalyst. (b) Fe2p scan XPS spectra of the FeN-TiO_2 catalyst. (c) The results of curve-fitting of the XPS spectra for O 1 s region of the N-TiO_2 catalyst. (d) The results of curve-fitting of the XPS spectra for O 1 s region of the FeN-TiO_2 catalyst.

$$FeN - TiO_2 \text{ or } N - TiO_2(h^+) + SO_3^{2-} \longrightarrow FeN - TiO_2 \text{ or } N - TiO_2 + SO_3^{-\bullet} \quad (13)$$

$$= Fe^{III} - OH + HSO_3^- \longrightarrow = Fe^{III} - OSO_2^- + H_2O \quad (14)$$

$$= Fe^{III} - OSO_2^- + h\nu \longrightarrow = Fe^{II} + SO_3^{-\bullet} \quad (15)$$

3.4. Influences of reaction parameters and stepwise addition strategy

A series of experiments was conducted by varying the initial concentration of sulfite ([sulfite]$_0$) from 0.1 to 2 mM to investigate its effect on DPA degradation and the results are shown in Fig. 4.a. As depicted in the inset of Fig. 4.a, the degradation rate increased markedly with the increment of [sulfite]$_0$ and reached an optimal value at 1 mM, whereas a slower decay was observed as the [sulfite]$_0$ further increased. Although the DPA decay increased significantly and reached the optimum

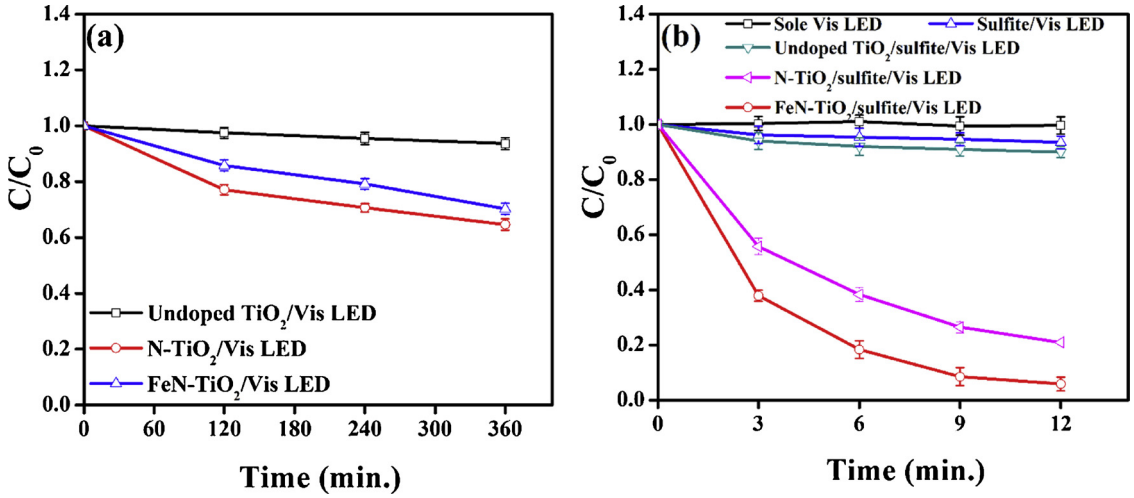

Fig. 3. (a) Role of different photocatalysts in DPA decay. (b) role of different processes in sulfite activation for DPA decay. ([DPA]$_0$ = 0.01 mM, [sulfite]$_0$ = 1 mM, [catalyst]$^{(a)}$ = 1 g/L, and [catalyst]$^{(b)}$ = 0.5 g/L). $^{(a)}$ Refers to the catalyst dosage at Fig. 3a and $^{(b)}$ refers to the catalyst dosage at Fig. 3b.

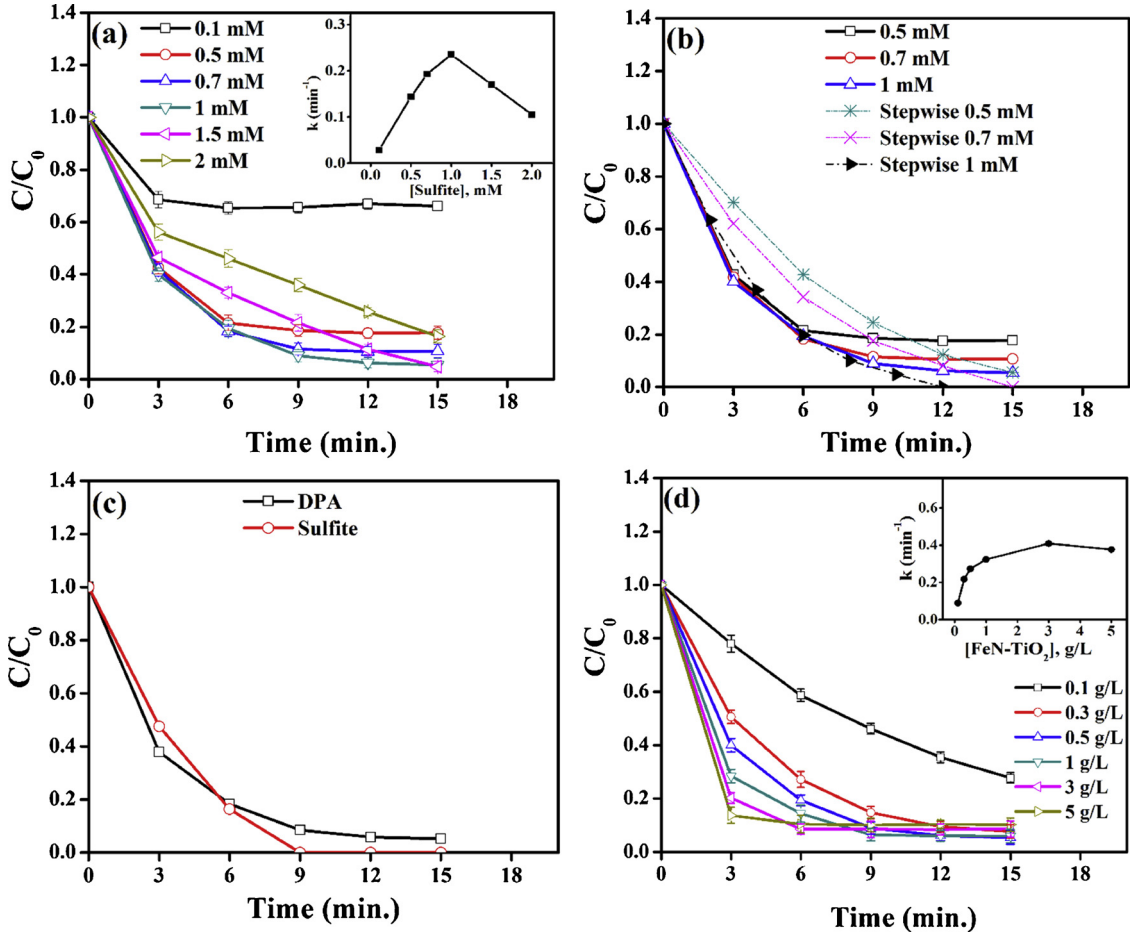

Fig. 4. (a) Influence of sulfite concentration on DPA decay (b) influence of stepwise addition of sulfite on DPA decay. (c) simultaneous degradation of DPA and sulfite. (d) influence of FeN-TiO_2 dosage on DPA decay. ($[DPA]_0$ = 0.01 mM, $[sulfite]_0$ = 1 mM, and $[FeN\text{-}TiO_2]$ = 0.5 g/L).

at $[sulfite]_0$ of 1 mM, the complete decay was not achieved, where the remaining [DPA] leveled off after 6 min. This retardation effect at a higher $[sulfite]_0$ or the leveling off phenomenon after an extended reaction time can be rationalized by the self-scavenging effect of $SO_3^{-\bullet}$ due to overdosed sulfite (Eqs. (16) and (17)) [45], and/or the competition of sulfite with the probe compound for the $^{\bullet}OH$ and $SO_4^{-\bullet}$ (Eqs. (18) and (19)) [15,46]. One possible way to minimize these effects is to reduce the peak concentration of radicals in the solution. Hence, stepwise addition of sulfite was sequentially performed by dividing the total dosage of sulfite into five small portions to lessen the futile depletion of $^{\bullet}OH$ and $SO_4^{-\bullet}$ occurring because of the scavenging effect. As presented in Fig. 4b, the results showed the decay of the DPA with various sulfite dosages under stepwise and one-batch addition modes. By using the one-batch addition, only 83%, 90%, and 95% of DPA was degraded in 15 min at $[sulfite]_0$ of 0.5, 0.7, and 1.0 mM, respectively; however, by using stepwise mode, the DPA decay significantly increased to 95%, 100%, and 100% in 12 min, respectively, by using the same total dosage of sulfite. Therefore, the stepwise addition strategy is environmentally and economically desirable since no additional amount of oxidant is required to enhance the degradation efficiency (i.e. complete degradation in shorter time).

Furthermore, the sulfite concentration was monitored during the degradation of DPA in the FeN-TiO_2/sulfite/Vis LED process and it was found that there was a simultaneous and complete depletion of sulfite (Fig. 4c), indicating that no sulfite residue was left in the solution after the reaction. Thus, it is a green technology without causing any environmental concern.

The influence of FeN-TiO_2 loading ($[FeN\text{-}TiO_2]$) on the DPA decay was explored by varying the $[FeN\text{-}TiO_2]$ from 0.1 to 5 g/L (Fig. 4d). Interestingly, the DPA degradation rate in the FeN-TiO_2/sulfite/Vis LED process increased significantly with the increment of $[FeN\text{-}TiO_2]$ from 0.1 to 3 g/L, while a retardation effect was observed at $[FeN\text{-}TiO_2]$ of 5 g/L. The lower decay rate at $[FeN\text{-}TiO_2]$ of 5 g/L may be ascribed to the deficiency of sulfite since the $[sulfite]_0$ was kept constant, where sulfite can be rapidly depleted at the beginning of the reaction, and no sufficient sulfite becomes available in the solution for generating radicals at the end of reaction. Another reason could be the light scattering induced by the overdose of the FeN-TiO_2 catalyst. In addition, the recombination of electrons and holes on the catalyst surface may be increased as the replenishment of oxygen and/or sulfite to the surface is not fast/good enough when the $[FeN\text{-}TiO_2]_0$ is overdosed. Furthermore, at very high $[FeN\text{-}TiO_2]$, the peak [radical] is boosted and creating more unwanted self-scavenging of radicals, as discussed before. Based on economic, practical, and environmental considerations, $[FeN\text{-}TiO_2]$ of 0.5 g/L and $[sulfite]_0$ of 1 mM were selected for the DPA decay in the following experiments.

$$SO_3^{-\bullet} + SO_3^{-\bullet} \longrightarrow S_2O_6^{2-} \quad (16)$$

$$SO_3^{-\bullet} + SO_3^{-\bullet} + H_2O \longrightarrow SO_4^{2-} + HSO_3^- + H^+ \quad (17)$$

$$HSO_3^- + SO_4^{-\bullet} \longrightarrow SO_4^{2-} + SO_3^{-\bullet} + H^+ \; k = (0.5 - 2) \times 10^9 M^{-1}s^{-1} \quad (18)$$

$$HSO_3^- + {}^{\bullet}OH \longrightarrow H_2O + SO_3^{-\bullet} \; k = 4.5 \times 10^9 M^{-1}s^{-1} \quad (19)$$

The effect of the initial DPA concentration ($[DPA]_0$) was also investigated at various concentrations (0.01 − 0.1 mM), while the other experimental conditions were kept constant at 0.5 g/L $[FeN\text{-}TiO_2]$ and 1 mM $[sulfite]_0$. As shown in Fig. 5, the DPA removal decreased from

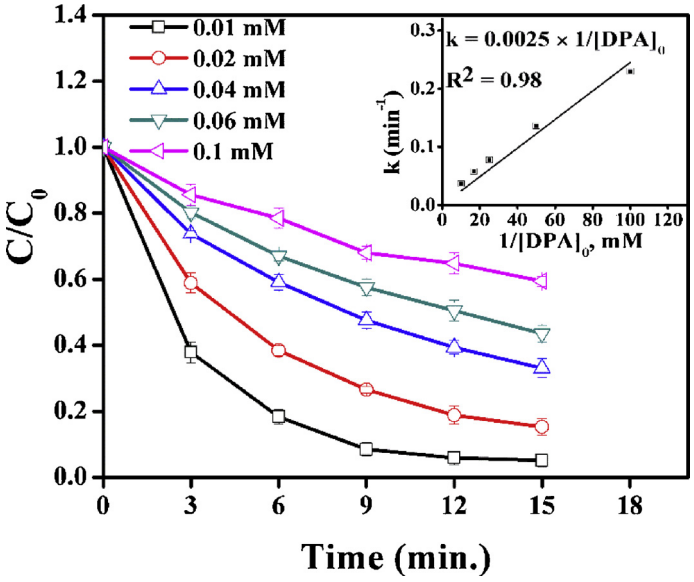

Fig. 5. Influence of initial concentration of DPA. ([sulfite]$_0$ = 1 mM and [FeN-TiO$_2$] = 0.5 g/L).

95% to 41% with the increment of [DPA]$_0$ from 0.01 mM to 0.1 mM. The DPA degradation followed the pseudo-first-order kinetics and a linear relationship was observed between k and 1/[DPA]$_0$ as shown in the inset of Fig. 5. Due to the constant [FeN-TiO$_2$], [sulfite]$_0$, and Vis LED light intensity, the generation of $^{\cdot}OH$ and $SO_4^{-\cdot}$ could be insufficient to degrade the DPA at higher concentrations. Furthermore, the formation of elevated concentrations of intermediates at higher [DPA]$_0$ may trigger a competition of $^{\cdot}OH$ and $SO_4^{-\cdot}$ between the intermediates and DPA, thereby causing retardation of DPA decay.

The effect of initial pH level (pH$_i$) on DPA degradation was explored in the FeN-TiO$_2$/sulfite/Vis LED process at various pH$_i$ from 2.7 to 11 as shown in Fig. 6a. It is worth noting that the DPA adsorption on the FeN-TiO$_2$ surface was proven insignificant for all investigated pH$_i$, suggesting that the adsorption was not a key factor for contributing to the DPA decay. As depicted in the inset of Fig. 6.a, the decay rate constant increased considerably with increasing pH$_i$ in the range (2.7–7.0), whereas a slight decrease was observed in the range (7.4–7.7), followed by a dramatic drop in the alkaline range (9.9–11.0), indicating that the neutral pH (pH$_i$ = 7.0) is the optimal condition. Based on Eqs. (20) and (21) [47], the sulfite exists as HSO_3^- at pH$_i$ 2.7–7.0, while SO_3^{2-} dominates in the solution at pH$_i$ 9.9–11.0. One the other hand, the pH$_{pzc}$ of FeN-TiO$_2$ catalyst is around 5.4 as aforementioned in Section 3.1, implying that the FeN-TiO$_2$ surface is positively charged at pH$_i$ 2.7–3.2 and negatively charged at pH$_i$ 7.0-11.0.

Therefore, the retardation in DPA decay at pH$_i$ 9.9–11.0 could be justified by the high electrostatic repulsion between the negatively charged FeN-TiO$_2$ and SO_3^{2-}. Besides, S-bonded metal-sulfitocomplexes can be formed at pH$_i$ higher than 9, thereby causing a drastic suppression in the DPA decay [10,48]. Nevertheless, O-bonded metal-sulfito complexes were reported to be formed at pH$_i$ range of 3–8 [10,48] consequently, the optimal decay was found at pH$_i$ = 7. It is speculated that the presence of HSO_3- at pH$_i$ = 7 instead of highly negative charged SO_3^{2-} at pH$_i$ 9.9–11.0 may lower the adverse effect of electrostatic repulsion with the catalyst. The slight decline at pH$_i$ 7.4–7.7 may be attributed to the initiation of sulfite speciation from HSO_3- to SO_3^{2-}.

$$SO_{2(aq.)} \Longleftrightarrow H^+ + HSO_3^-,\ pK_a = 1.86 \quad (20)$$

$$HSO_3^- \Longleftrightarrow H^+ + SO_3^{2-},\ pK_a = 7.2 \quad (21)$$

Hence, it can be inferred that pH can influence the sulfite speciation and surface complexation between FeN-TiO$_2$ and sulfite. In addition, the FeN-TiO$_2$/sulfite/Vis LED process was proven efficient for DPA decay under neutral conditions, suggesting its feasibility for wastewater treatment. Since pH$_i$ 7.7 exhibited an acceptable efficiency without pH adjustment, the following tests were conducted at pH$_i$ 7.7 (unadjusted) due to practical considerations.

Meanwhile, the pH variation during the DPA decay was monitored for the studied pH range, and the results are presented in Fig. 6b. Obviously, no appreciable change of solution pH$_i$ was observed for extreme acidic pH$_i$ (2.7–3.2) and alkaline pH$_i$ (9.9–11) due to the strong buffer capacity. However, a sharp drop in pH level was induced at pH$_i$ (7.0–7.7), where the pH declined dramatically in the first 6 min and then stabilized due to sulfite depletion. This is because of the generation of protons as a byproduct according to Eqs. (5), (6), and (12), and the formation of acidic intermediates during the DPA decay.

3.5. Leaching of Fe ions and role of homogenous reaction

In order to investigate the leaching of Fe ions from the solid catalyst to bulk solution, total Fe ions were measured after the photocatalytic reaction at various pH$_i$ as shown in Table S2 (Supporting Information). As expected, the concentrations of leached Fe ions were below the detection limit of the instrument at pH$_i$ 7.4–11 (< 0.5 mg/L). The low leaching at extreme alkaline pH (pH$_i$ 9.9 and pH$_i$ 11.0) could be as a result of the precipitation of iron hydroxides that may remain attached to the catalyst surface. However, a slight increment was observed at pH$_i$ 2.7–7.0 owing to the exchange of Fe ions with H^+, where Fe concentrations were detected to be 1.21, 0.70, and 0.58 mg/L at pH$_i$ 2.7, 3.2, and 7.0, respectively. The insignificant Fe leaching at neutral pH$_i$ 7.0 can be rationalized by the decrease in final pH after the reaction as referred as pH$_f$ in Table S2. It was reported that the recommended limit of Fe in reclaimed water for irrigation is 5.0 mg/L [10], implying that the FeN-TiO$_2$/sulfite/Vis LED process is favorable from the environmental point of view.

The leaching of Fe ions to the environment however can contribute to the photocatalytic processes via a homogeneous sulfite activation (if any), thereby potentially affecting the safety of effluent. The role of homogeneous reactions in DPA decay was therefore investigated at various pH$_i$. The DPA solution was adjusted to the required pH value, then the FeN-TiO$_2$ catalyst was added and the suspension was stirred for 30 min. Afterward, the catalyst was removed by filtration and sulfite was added to the supernatant to initiate the photocatalytic reaction. As illustrated in Fig. 6c, the results showed that the DPA decay was negligible (2%–5%) for all investigated pH$_i$ except pH$_i$ 7.0 and pH$_i$ 7.4, at

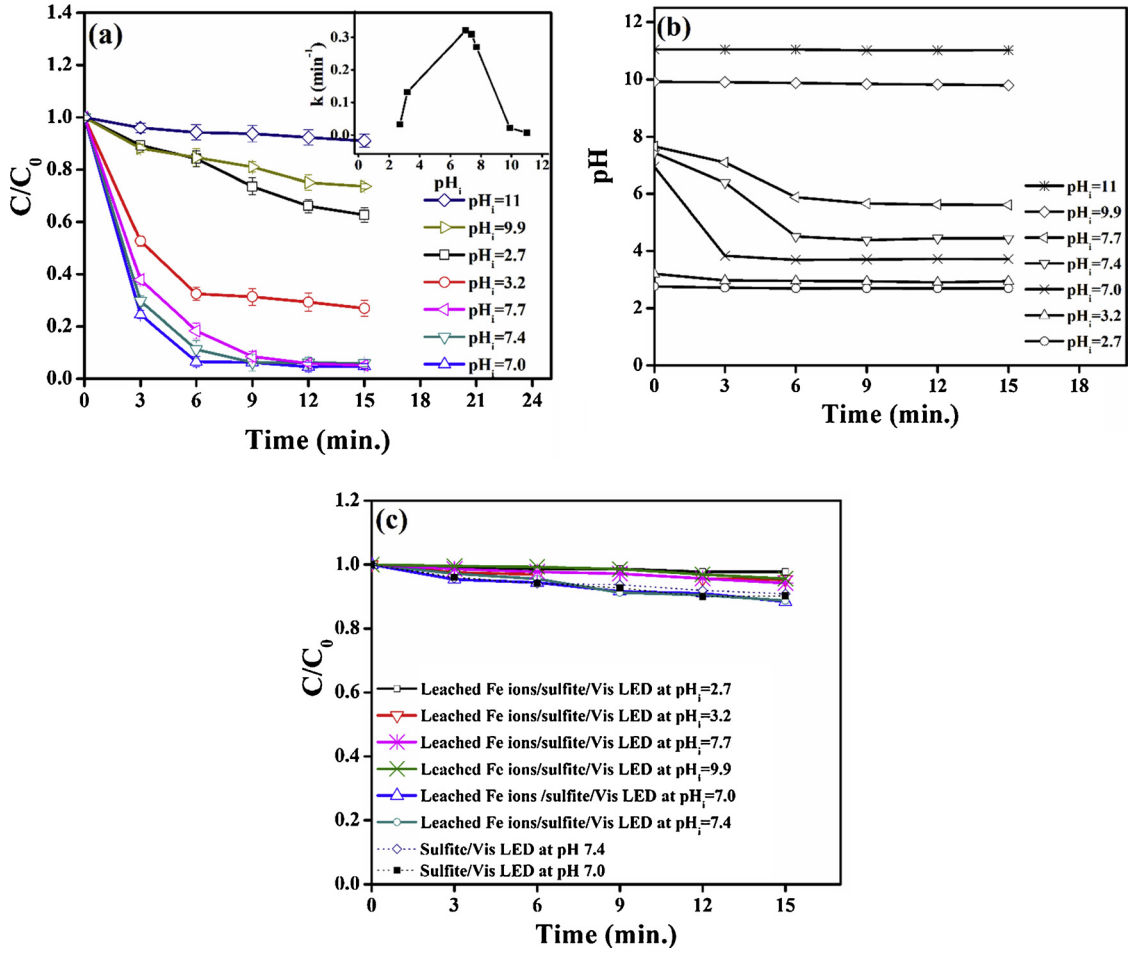

Fig. 6. (a) Influence of solution pH on DPA decay. (b) the pH change during DPA decay. (c) role of homogeneous reaction in the catalytic oxidation of DPA. ($[DPA]_0$ = 0.01 mM, $[sulfite]_0$ = 1 mM, and [FeN-TiO_2] = 0.5 g/L).

which about 13% decay was achieved. It should be pointed out that the contribution of homogeneous reaction was negligible at acidic pH despite their higher leaching rate. This can be ascribed to the inefficiency of Fe ions for sulfite activation under Vis LED in the absence of FeN-TiO_2.

To examine the plausible reason for the higher decay at pH_i 7.0 and pH_i 7.4, the DPA decay was investigated in sulfite/Vis LED process under the same experimental conditions without the catalyst involvement as shown in Fig. 6c. Interestingly, the DPA decay showed a similar efficiency in the sole sulfite/Vis LED process compared to that of the leached FeN-TiO_2/sulfite/Vis LED. This indicates that the DPA decay was mainly due to sole sulfite activation under Vis LED rather than the involvement of leached Fe ions. Therefore, the contribution of homogeneous sulfite activation to the FeN-TiO_2/sulfite/Vis LED process is negligible; and the DPA decay is mainly induced by a heterogeneous reaction mechanism on the catalyst surface.

3.6. Reusability and stability of FeN-TiO_2

To examine the chemical stability of FeN-TiO_2, the DPA decay was investigated in the FeN-TiO_2/sulfite/Vis LED process for five successive cycles (Fig. 7). The used catalyst was separated, rinsed with ultrapure water, dried overnight at 80 °C. The catalyst was then added to the DPA solution without supplementing any fresh amount and the photocatalytic reaction was initiated by addition of sulfite. Surprisingly, no reduction in the catalyst performance was observed after five cycles; instead, the DPA decay was significantly improved after successive usage of the catalyst. For instance, the DPA decay increased from 95% within 15 min after 1st cycle to about 100% in 6 min after 5th cycle. This is likely due to activation of catalyst surface by the continuous wetting after each reuse [9,49]. The leaching of total Fe ions was also explored after each cycle and the results revealed that total Fe concentrations were lower than the detection limit of the instrument (< 0.5 mg/L) (data not shown). Therefore, the high stability of FeN-TiO_2 may be ascribed to the negligible leaching of Fe after each reuse. Compared to N-TiO_2 reusability results in our previous study [9], the impregnation of Fe ions on the N-TiO_2 not only enhanced heterogeneous sulfite activation but also maintained long-term stability of the catalyst.

3.7. Reactive species and reaction mechanisms

3.7.1. Mechanism of heterogeneous sulfite activation

The mechanism of sulfite activation by FeN-TiO_2 under Vis LED can be induced as aforementioned described in Eqs. (7)–(15) [10,15,20] and Eqs. (2)–(6) [10,15,16]. The FeN-TiO_2 can be activated under Vis LED irradiation to give birth to electrons and holes (Eq. (7)), followed by the subsequent reactions of electrons and holes with dissolved oxygen and sulfite ions, respectively (Eqs. (8), (12) and (13)). The reaction of electrons with adsorbed oxygen on the catalyst surface leads to the generation of superoxide radicals, which undergo further reactions and eventually produce $^{\cdot}OH$ (Eqs. (8)–(11)). While the holes can be reduced by sulfite ions to generate sulfite radicals (Eqs. (12) and (13)). Afterward, the formation of metal sulfitocomplexes can be induced by the reaction of FeN-TiO_2 with sulfite ions under Vis LED irradiation through surface hydroxyl groups, leading to the generation of additional sulfite radicals (Eqs. (14) and (15)). The generated sulfite

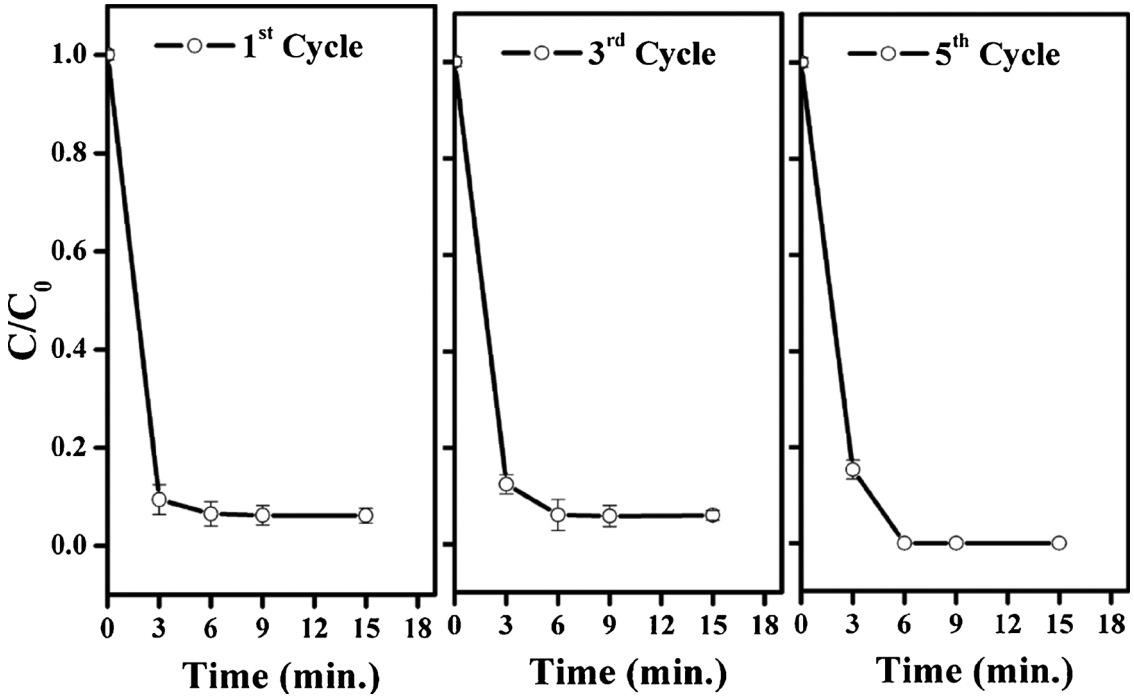

Fig. 7. DPA degradation in five continuous reuses. ([sulfite]$_0$ = 1 mM, and [FeN-TiO$_2$] = 3 g/L).

radicals can react with dissolved oxygen to produce $SO_5^{-\cdot}$ species, which can give $SO_4^{-\cdot}$ by the direct reaction with another molecule of $SO_5^{-\cdot}$ (Eq. (3)) and/or by the reaction with sulfite ions (Eqs. (4) and (5)). Furthermore, $SO_4^{-\cdot}$ can react with H_2O, producing $^{\cdot}OH$ (Eq. (6)).

The roles of sulfite, types of reactive species, and possible formation pathways were elucidated by radical scavenging tests, and the results are shown in Fig. 8a. Chloroform was used as a quencher to investigate the contribution of superoxide radicals to the generation of $^{\cdot}OH$ ($k_{chloroform,\ \dot{O}2-} = 3 \times 10^{10}\ M^{-1}\ s^{-1}$) [50,51]. The DPA decay declined by about 4% in the presence of chloroform, indicating the negligible role of $^{\cdot}O_2^-$ in the generation of $^{\cdot}OH$ species. This is rationale since the FeN-TiO$_2$/Vis LED process is inefficient for DPA decay in the absence of sulfite as discussed in Section 3.2. Although $SO_3^{-\cdot}$ can be generated as illustrated in the proposed equations, several literatures reported its weak contribution to the photocatalytic reaction due to its low oxidation potential ($E_{SO3-}{}^{\cdot}$) = 0.63 V) [10,52]. However, a recent study suggested that the sulfite radicals were the active species for degradation of methyl orange in the BiOBr/sulfite system [14]. The contribution of $SO_3^{-\cdot}$ was therefore examined in the absence of oxygen (bubbling nitrogen) to investigate its role in the DPA decay. Obviously, the DPA degradation was strongly suppressed after purging nitrogen into the solution, implying the insignificant role of $SO_3^{-\cdot}$ in the photocatalytic reaction. Consequently, it was speculated that $SO_3^{-\cdot}$ could undergo oxidation to $SO_5^{-\cdot}$, which accordingly generates $SO_4^{-\cdot}$ (Eqs. (2)–(5)). Furthermore, $SO_4^{-\cdot}$ could react with H_2O, giving rise to $^{\cdot}OH$ (Eq. (6)). To verify these hypotheses, ethanol and ter-butyl alcohol (TBA) with different initial concentrations were applied as quenchers for $^{\cdot}OH$ and $SO_4^{-\cdot}$ in the FeN-TiO$_2$/sulfite/Vis LED process. Ethanol is capable of scavenging both $^{\cdot}OH$ and $SO_4^{-\cdot}$ ($k_{Ethanol,\ \dot{O}H}$ = (1.8–2.8) × 10^9 M^{-1} s^{-1}, $k_{Ethanol,\ SO4-}{}^{\cdot}$ = (1.6–7.7) × 10^7 M^{-1} s^{-1} [52,53]), whereas TBA is used as a scavenger for $^{\cdot}OH$ ($k_{TBA,\ \dot{O}H}$ = (3.8–7.6) × 10^8 M^{-1} s^{-1}, $k_{TBA,\ SO4-}{}^{\cdot}$ = (4.0–9.1) × 10^5 M^{-1} s^{-1} [53,54]). The DPA degradation dropped from 95% to 21%, 5%, and 4% in the presence of 10 mM, 50 mM, and 100 mM Ethanol, respectively. While the DPA decay declined to 43%, 29%, and 15% as the TBA concentration increased to 100 mM, 200 mM, and 600 mM,

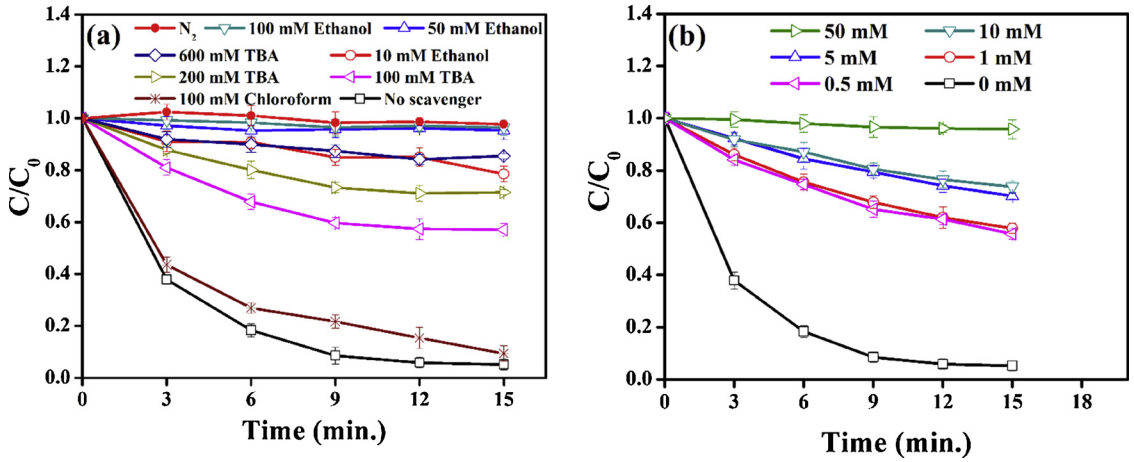

Fig. 8. (a) Influence of radicals' scavengers on DPA degradation. (b) Influence of phosphate ions on DPA degradation. ([DPA]$_0$ = 0.01 mM, [sulfite]$_0$ = 1 mM, and [FeN-TiO$_2$] = 0.5 g/L).

respectively. This implies that $^{\cdot}OH$ and $SO_4^{-\cdot}$ are the active radicals for the DPA degradation in the process.

3.7.2. Role of surface hydroxyl groups and identification of active sites

To elucidate the role of surface hydroxyl groups in the formation of metal sulfito-complexes as described in Eqs. (14) and (15), competitive experiments were conducted by using phosphate, a strong chelating ligand. Several investigations reported that phosphate has a strong ability to chelate metals via its affinity for hydroxyl groups on the catalyst surface [10,55]. Phosphate ions were therefore added to the reaction solution and the efficiency of FeN-TiO_2/sulfite/Vis LED process was investigated at various [phosphate] (Fig. 8b), where the DPA degradation dramatically inhibited from 95% to 4% with the continuous increase of [phosphate] from 0 to 50 mM. This can be ascribed to the competition of phosphate ions with sulfite ions in complexing iron, thereby suppressing the formation of metal sulfito-complexes which are precursors of reactive radicals. Although the phosphate ions were reported to have a scavenging effect on both $^{\cdot}OH$ and $SO_4^{-\cdot}$, the retardation effect caused by 5 mM phosphate was much higher than that of 100 mM TBA. This indicates that the radical scavenging effect of phosphate ions may not be the main rationale, however, another factor could be the replacement of surface hydroxyl groups by phosphate ions.

To verify the regeneration of Fe (II), and to find out the primary functional sites in the FeN-TiO_2/sulfite/Vis LED process, the XPS analysis was utilized to give a clear insight into the surface composition of the FeN-TiO_2 powder before and after the reaction (Fig. 9). The peak values at 709.5 and 710.5 eV are corresponding to Fe (II)$2p_{3/2}$ and Fe (III)$2p_{3/2}$, respectively. The Fe (II)$2p_{3/2}$ peak increased from 45.5% before reaction to 53.12% after reaction, whereas Fe (III)$2p_{3/2}$ peak decreased from 54.5% before reaction to 46.88% after reaction (Table S3 (Supporting Information)). This indicates that part of Fe (III) on the FeN-TiO_2 surface was reduced to Fe (II) during the reaction in Eq. (15). Thus, the surface hydroxyl site of the FeN-TiO_2 was further confirmed to be an important active site in the FeN-TiO_2/sulfite/Vis LED process, where it can lead to the formation of metal sulfito-complexes (Eq. (14)), which in turn can be decomposed using Vis LED irradiation, leading to the reduction of Fe (III) to Fe (II) and generation of $SO_3^{-\cdot}$ species (Eq. (15)).

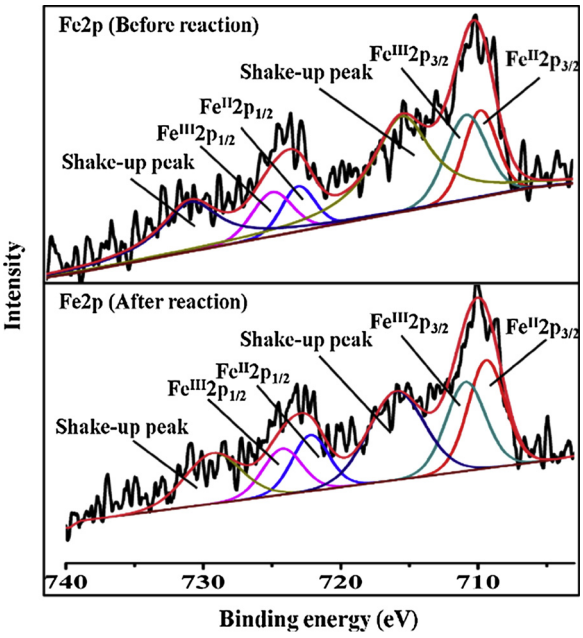

Fig. 9. XPS spectrum of Fe2p of the FeN-TiO_2 catalyst before and after reaction.

3.8. Mineralization and degradation products

3.8.1. Mineralization

Mineralization of DPA was evaluated in the FeN-TiO_2/sulfite/Vis LED process by investigating total organic carbon (TOC) levels. As illustrated in Fig. 10, 53% TOC reduction was observed in the FeN-TiO_2/sulfite/Vis LED process when DPA was fully degraded. This result totally overwhelms the poor TOC reductions as reported from previous sulfite studies due to the generation of sulfate adduct [35,56] or the scavenging of holes and $^{\cdot}OH$ by sulfite [14]. Therefore, our results indicate that the FeN-TiO_2/sulfite/Vis LED process could be a very promising approach not only for treatment of organic pollutants in wastewater but also for elimination of generated intermediates through sulfite activation.

3.8.2. Identification of reaction intermediates

The DPA degradation pathway was examined in the FeN-TiO_2/sulfite/Vis LED process by exploring reaction intermediates generated in the process. A total of thirty reaction intermediates were recognized as illustrated in Scheme 1. The information of DPA and its detected intermediates including chemical structure, formula, and mass over charge ratio (m/z) is shown in Table S4 (Supporting Information) and the corresponding MS spectrums are presented in Fig. S2 (Supporting Information). In comparison with previous investigations on DPA degradation, twenty-four new intermediates (indicated within brackets) were recognized in this study for the first time (i.e. only six intermediates (Int 1, 2, 3, 4, 9, and 10) were reported in previous studies [5,6]. The degradation mechanism of DPA involves four main routes including N-dealkylation, hydroxylation of the aromatic cycle, isomerization, and rupture of benzene ring linkage.

The N-dealkylation can be induced by the radicals' attack on the N-terminus methyl group, leading to the generation of Int 1 which is prone to further oxidation, yielding Int 2, Int 3, and Int 4. The Int 4 underwent further demethylation through alkylic oxidation of the second N-methyl group, producing Int 5, Int 6, Int 7, and Int 8.

The direct hydroxylation of DPA can be provoked by the attack of $^{\cdot}OH$ on the aromatic ring, leading to the formation of two hydroxylated isomers (Int 9 and Int 10), accompanied by the N-dealkylation of terminus methyl groups, which results in several hydroxylated isomers (from Int 11 to Int 21). The hydroxylated isomers were distinguished based on their yield, where the para-position is more nucleophilic and accessible than the ortho-position [5]. Although multi-hydroxylated compounds were commonly detected in many advanced oxidation processes (AOPs) due to the excessive generation of $^{\cdot}OH$ species at the beginning of reactions [8,57,58], no di or tri-hydroxylated compounds were identified in this study, implying that the $^{\cdot}OH$ species generated in the FeN-TiO_2/sulfite/Vis LED process were utilized efficiently (remark: if the mineralization is possible for the adopted AOP, the formation of multi-hydroxylated intermediates is not a desirable process, because of the waste of valuable radicals).

Another possible pathway can occur by the breakage of CH—C bond of DPA, causing the rupture of benzene ring linkage, thereby generating Int 22. Analogously to N-dealkylation mechanism discussed above, the Int 22 is susceptible to subsequent alkylic oxidation, producing the compounds from Int 23 to Int 30. The detection of further intermediates (Int 23 to Int 30) confirms the emergence of Int 22 through the breakage of CH—C bond.

Interestingly, the rupture of benzene ring linkage along with DPA decay was never reported before, indicating that the FeN-TiO_2/sulfite/Vis LED process could be conducive for diminishing the toxicity of organic pollutants via mineralization. Furthermore, no sulfate adducts were detected in this study as reported in most sulfite-based processes. This observation is consistent with the better TOC removal achieved using the FeN-TiO_2/sulfite/Vis LED process, where the absence of sulfate adducts minimizes the undesirable radicals' depletion for the generation of such futile intermediates. Therefore, the mechanism

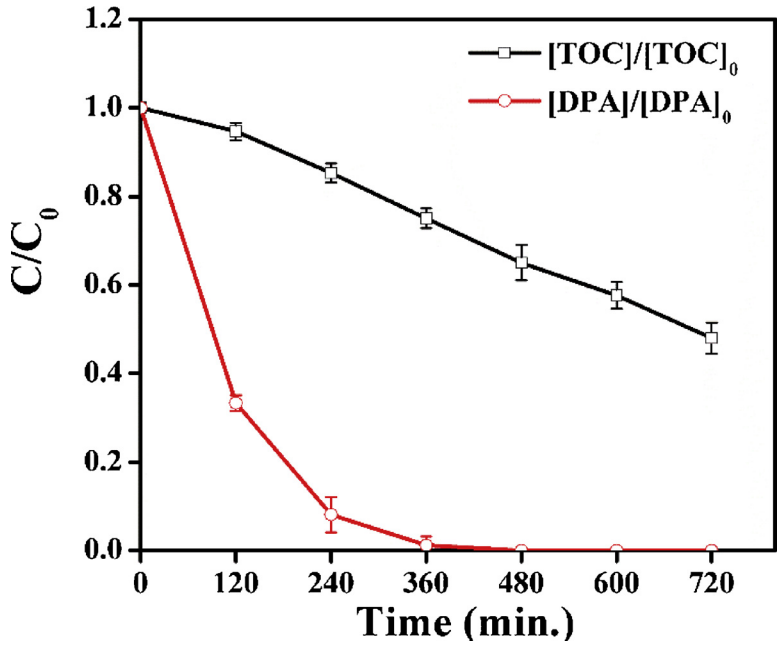

Fig. 10. Simultaneous TOC measurements and DPA degradation in the FeN-TiO_2/sulfite/Vis LED process. ([sulfite]$_0$ = 10.4 mM, [FeN-TiO_2] = 2 g/L, [DPA]$_0$ = 0.1 mM).

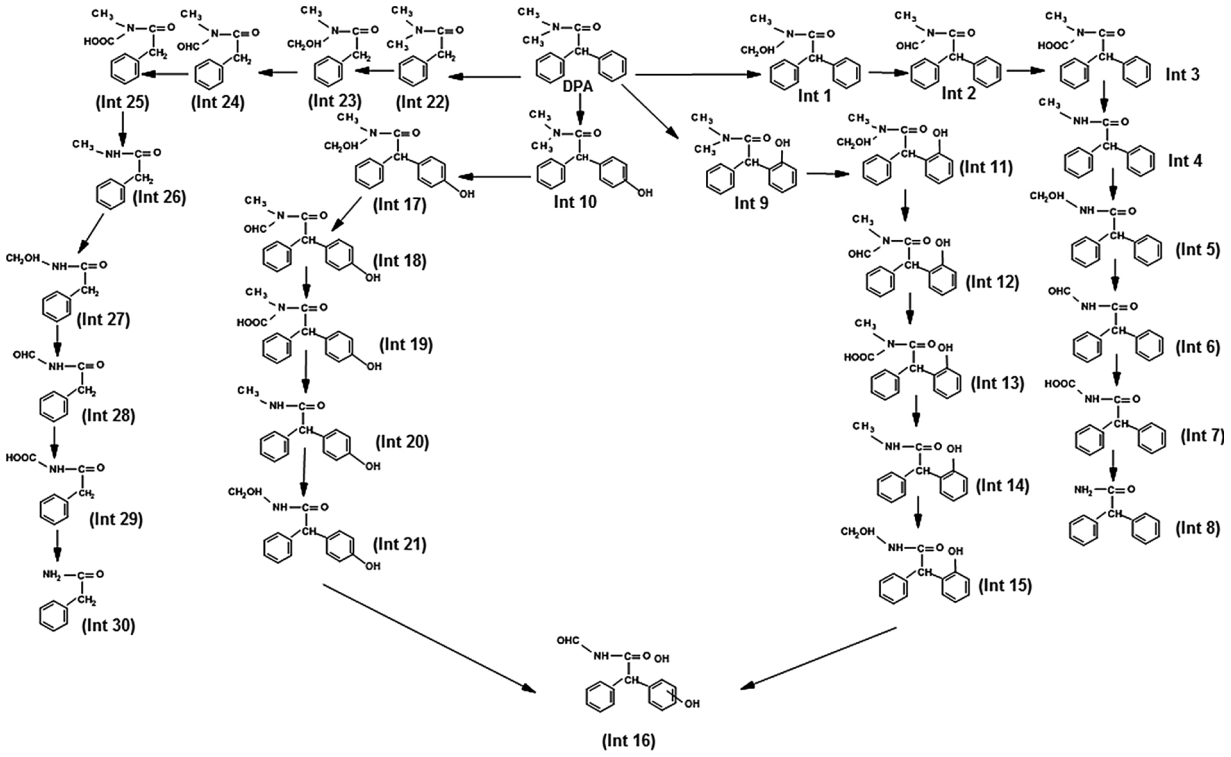

Scheme 1. The proposed degradation routes of DPA in the FeN-TiO_2/sulfite/Vis LED process.

confirms that FeN-TiO_2/sulfite/Vis LED is a green technology for degradation of organic pollutants.

4. Conclusion

In summary, the new photocatalyst FeN-TiO_2, compared to N-TiO_2, resulted in an enhanced efficiency for DPA decay through sulfite activation under vis LED. The leaching of Fe-ions from the FeN-TiO_2 catalyst was negligible, where the leached Fe concentrations were lower than the recommended limit of Fe in reclaimed water for irrigation for all investigated pH values (2.7–11). Surprisingly, its performance was even improved after repeated usage. The radical scavenging experiments elucidated that $^{\cdot}O_2^-$ and $SO_3^{-\cdot}$ have a negligible role in the DPA degradation, whereas $^{\cdot}OH$ and $SO_4^{-\cdot}$ are the dominating radicals. 53% TOC reduction was achieved in the FeN-TiO_2/sulfite/Vis LED process. Thirty intermediates were detected during DPA decay through four major routes including N-dealkylation, hydroxylation of the aromatic cycle, isomerization, and rupture of benzene ring linkage. No sulfate adducts were detected in the process and a new pathway through the rupture of benzene ring linkage was observed for the first time. The

obtained results suggest that the proposed FeN-TiO_2/sulfite/Vis LED is a green and environmentally benign process.

Acknowledgments

This study was financially funded by a grant from the Hong Kong Polytechnic University (project no. RUP5). The authors acknowledge the environmental officers in the Research Facility, Chemical and Environmental Analysis (UCEA), the Hong Kong Polytechnic University for their technical help in the usage of UPLC-ESI-MS.

Appendix A. Supplementary data

Supplementary material related to this article can be found, in the online version, at doi:https://doi.org/10.1016/j.apcatb.2018.11.085.

References

[1] X. Wu, M. Li, Y. Long, R. Liu, Y. Yu, H. Fang, Adsorption, mobility and degradation of diphenamid in chinese soils, KSCE J. Civ. Eng. 16 (2012) 547–553.
[2] A. Czescik, D.L. Malo, M. Duart, L.L. Zamora, G.A. Fos, J.M. Calatayud, Photo-induced chemiluminescence-based determination of diphenamid by using a multicommuted flow system, Talanta 73 (2007) 718–725.
[3] G. Jones, H. Dubey, J. Freeman, Persistence of diphenamid in tobacco field soils, Weeds 12 (1964) 313–315.
[4] T. Sheets, C. Harris, Herbicide residues in soils and their phytotoxicities to crops grown in rotations, Residue Rev. Springer, 1965, pp. 119–140.
[5] H.-c. Liang, X.-z. Li, Y.-h. Yang, K.-h. Sze, Comparison of the degradations of diphenamid by homogeneous photolysis and heterogeneous photocatalysis in aqueous solution, Chemosphere 80 (2010) 366–374.
[6] M.A. Rahman, M. Muneer, D. Hahnemann, Photocatalysed degradation of a herbicide derivative, diphenamid in aqueous suspension of titanium dioxide, J. Adv. Oxid. Technol. 6 (2003) 100–108.
[7] C. Casado, R. Timmers, A. Sergejevs, C. Clarke, D. Allsopp, C. Bowen, R. van Grieken, J. Marugán, Design and validation of a LED-based high intensity photocatalytic reactor for quantifying activity measurements, Chem. Eng. J. 327 (2017) 1043–1055.
[8] A. Abdelhaleem, W. Chu, Monuron photodegradation using peroxymonosulfate activated by non-metal-doped TiO_2 under visible LED and the modeling via a parallel-serial kinetic approach, Chem. Eng. J. (2018).
[9] A. Abdelhaleem, W. Chu, Photodegradation of 4-chlorophenoxyacetic acid under visible LED activated N-doped TiO_2 and the mechanism of stepwise rate increment of the reused catalyst, J. Hazard. Mater. 338 (2017) 491–501.
[10] Y. Huang, C. Han, Y. Liu, M.N. Nadagouda, L. Machala, K.E. O'Shea, V.K. Sharma, D.D. Dionysiou, Degradation of atrazine by $Zn_xCu_{1-x}Fe_2O_4$ nanomaterial-catalyzed sulfite under UV–vis light irradiation: green strategy to generate $SO_4^{-\bullet}$, Appl. Catal. B 221 (2018) 380–392.
[11] H. Lin, J. Wu, H. Zhang, Degradation of clofibric acid in aqueous solution by an EC/Fe^{3+}/PMS process, Chem. Eng. J. 244 (2014) 514–521.
[12] J. Zhang, L. Zhu, Z. Shi, Y. Gao, Rapid removal of organic pollutants by activation sulfite with ferrate, Chemosphere 186 (2017) 576–579.
[13] Y. Yu, S. Li, X. Peng, S. Yang, Y. Zhu, L. Chen, F. Wu, G. Mailhot, Efficient oxidation of bisphenol A with oxysulfur radicals generated by iron-catalyzed autoxidation of sulfite at circumneutral pH under UV irradiation, Environ. Chem. Lett. 14 (2016) 527–532.
[14] W. Deng, H. Zhao, F. Pan, X. Feng, B. Jung, A. Abdel-Wahab, B. Batchelor, Y. Li, Visible-light-d photocatalytic degradation of organic water pollutants promoted by sulfite addition, Environ. Sci. Technol. 51 (2017) 13372–13379.
[15] L. Zhang, L. Chen, M. Xiao, L. Zhang, F. Wu, L. Ge, Enhanced decolorization of orange II solutions by the Fe (II)–sulfite system under xenon lamp irradiation, Ind. Eng. Chem. Res. 52 (2013) 10089–10094.
[16] L. Chen, X. Peng, J. Liu, J. Li, F. Wu, Decolorization of Orange II in aqueous solution by an Fe (II)/sulfite system: replacement of persulfate, Ind. Eng. Chem. Res. 51 (2012) 13632–13638.
[17] A.K. Sharma, A. Singh, R. Mehta, S. Sharma, S. Bansal, K. Gupta, Kinetics of copper (II)-catalyzed oxidation of S (IV) by atmospheric oxygen in ammonia buffered solutions, Int. J. Chem. Kinet. 43 (2011) 379–392.
[18] A.K. Sharma, P.K. Mudgal, S. Bansal, K. Gupta, Kinetics of the simultaneous oxidation of Nickel (II) and Sulfur (IV) by oxygen in alkaline medium in Ni (II)–Sulfur (IV)–O2 system, Int. J. Chem. Kinet. 42 (2010) 464–478.
[19] D. Zhou, Y. Yuan, S. Yang, H. Gao, L. Chen, Roles of oxysulfur radicals in the oxidation of acid orange 7 in the Fe (III)–sulfite system, J. Sulfur Chem. 36 (2015) 373–384.
[20] Y. Guo, X. Lou, C. Fang, D. Xiao, Z. Wang, J. Liu, Novel photo-sulfite system: toward simultaneous transformations of inorganic and organic pollutants, Environ. Sci. Technol. 47 (2013) 11174–11181.
[21] Y. Yao, H. Chen, J. Qin, G. Wu, C. Lian, J. Zhang, S. Wang, Iron encapsulated in boron and nitrogen codoped carbon nanotubes as synergistic catalysts for Fenton-like reaction, Water Res. 101 (2016) 281–291.
[22] J. Zhu, W. Zheng, B. He, J. Zhang, M. Anpo, Characterization of Fe–TiO_2 photocatalysts synthesized by hydrothermal method and their photocatalytic reactivity for photodegradation of XRG dye diluted in water, J. Mol. Catal. A Chem. 216 (2004) 35–43.
[23] A. Di Paola, G. Marci, L. Palmisano, M. Schiavello, K. Uosaki, S. Ikeda, B. Ohtani, Preparation of polycrystalline TiO_2 photocatalysts impregnated with various transition metal ions: characterization and photocatalytic activity for the degradation of 4-nitrophenol, J. Phys. Chem. B 106 (2002) 637–645.
[24] K. Nagaveni, M. Hegde, G. Madras, Structure and photocatalytic activity of $Ti_{1-x}M_xO_2 \pm \delta$ (M= W, V, Ce, Zr, Fe, and Cu) synthesized by solution combustion method, J. Phys. Chem. B 108 (2004) 20204–20212.
[25] J. Zhou, M. Takeuchi, A.K. Ray, M. Anpo, X. Zhao, Enhancement of photocatalytic activity of P_{25} TiO_2 by vanadium-ion implantation under visible light irradiation, J. Colloid Interface Sci. 311 (2007) 497–501.
[26] M.M. Mohamed, M.M. Al-Esaimi, Characterization, adsorption and photocatalytic activity of vanadium-doped TiO_2 and sulfated TiO_2 (rutile) catalysts: degradation of methylene blue dye, J. Mol. Catal. A Chem. 255 (2006) 53–61.
[27] Q. Wang, S. Xu, F. Shen, Preparation and characterization of TiO2 photocatalysts co-doped with iron (III) and lanthanum for the degradation of organic pollutants, Appl. Surf. Sci. 257 (2011) 7671–7677.
[28] W. Choi, A. Termin, M.R. Hoffmann, The role of metal ion dopants in quantum-sized TiO_2: correlation between photoreactivity and charge carrier recombination dynamics, J. Phys. Chem. 98 (1994) 13669–13679.
[29] Z. Ambrus, N. Balázs, T. Alapi, G. Wittmann, P. Sipos, A. Dombi, K. Mogyorósi, Synthesis, structure and photocatalytic properties of Fe (III)-doped TiO_2 prepared from $TiCl_3$, Appl. Catal. B 81 (2008) 27–37.
[30] C. Wang, Q. Li, R. Wang, Synthesis and characterization of mesoporous iron-doped TiO_2, J. Mater. Sci. 39 (2004) 1899–1901.
[31] Y. Cong, J. Zhang, F. Chen, M. Anpo, D. He, Preparation, photocatalytic activity, and mechanism of nano-TiO_2 co-doped with nitrogen and iron (III), J. Phys. Chem. C 111 (2007) 10618–10623.
[32] M. Piumetti, F.S. Freyria, M. Armandi, F. Geobaldo, E. Garrone, B. Bonelli, Fe-and V-doped mesoporous titania prepared by direct synthesis: Characterization and role in the oxidation of AO7 by H_2O_2 in the dark, Catal. Today 227 (2014) 71–79.
[33] T. Ohno, Z. Miyamoto, K. Nishijima, H. Kanemitsu, F. Xueyuan, Sensitization of photocatalytic activity of S-or N-doped TiO_2 particles by adsorbing Fe^{3+} cations, Appl. Catal. A Gen. 302 (2006) 62–68.
[34] L. Singh, P. Rekha, S. Chand, Cu-impregnated zeolite Y as highly active and stable heterogeneous Fenton-like catalyst for degradation of Congo red dye, Sep. Purif. Technol. 170 (2016) 321–336.
[35] Z. Liu, S. Yang, Y. Yuan, J. Xu, Y. Zhu, J. Li, F. Wu, A novel heterogeneous system for sulfate radical generation through sulfite activation on a $CoFe_2O_4$ nanocatalyst surface, J. Hazard. Mater. 324 (2017) 583–592.
[36] X. Wang, K. Wang, K. Feng, F. Chen, H. Yu, J. Yu, Greatly enhanced photocatalytic activity of TiO2− xNx by a simple surface modification of Fe (III) cocatalyst, J. Mol. Catal. A Chem. 391 (2014) 92–98.
[37] F. Dong, H. Wang, Z. Wu, J. Qiu, Marked enhancement of photocatalytic activity and photochemical stability of N–doped TiO_2 nanocrystals by Fe^{3+}/Fe^{2+} surface modification, J. Colloid Interface Sci. 343 (2010) 200–208.
[38] D. Dolat, S. Mozia, R. Wróbel, D. Moszyński, B. Ohtani, N. Guskos, A. Morawski, Nitrogen-doped, metal-modified rutile titanium dioxide as photocatalysts for water remediation, Appl. Catal. B 162 (2015) 310–318.
[39] H. Yu, H. Irie, Y. Shimodaira, Y. Hosogi, Y. Kuroda, M. Miyauchi, K. Hashimoto, An efficient visible-light-sensitive Fe (III)-grafted TiO_2 photocatalyst, J. Phys. Chem. C 114 (2010) 16481–16487.
[40] M. Nishikawa, Y. Mitani, Y. Nosaka, Photocatalytic reaction mechanism of Fe (III)-grafted TiO_2 studied by means of ESR spectroscopy and chemiluminescence photometry, J. Phys. Chem. C 116 (2012) 14900–14907.
[41] S.B. Rawal, H.J. Kim, W.I. Lee, Enhanced visible-light photocatalytic properties of Fe^{3+}-grafted N-doped TiO_2 nanoporous spheres, Appl. Catal. B 142 (2013) 458–464.
[42] G.K. Mor, H.E. Prakasam, O.K. Varghese, K. Shankar, C.A. Grimes, Vertically oriented Ti− Fe− O nanotube array films: toward a useful material architecture for solar spectrum water photoelectrolysis, Nano Lett. 7 (2007) 2356–2364.
[43] N. Banić, B. Abramović, J. Krstić, D. Šojić, D. Lončarević, Z. Cherkezova-Zheleva, V. Guzsvány, Photodegradation of thiacloprid using Fe/TiO_2 as a heterogeneous photo-Fenton catalyst, Appl. Catal. B 107 (2011) 363–371.
[44] M. Litter, J.A. Navio, Photocatalytic properties of iron-doped titania semiconductors, J. Photochem. Photobiol. A: Chem. 98 (1996) 171–181.
[45] Y. Gu, W. Dong, C. Luo, T. Liu, Efficient reductive decomposition of perfluorooctanesulfonate in a high photon flux UV/sulfite system, Environ. Sci. Technol. 50 (2016) 10554–10561.
[46] J. Xu, W. Ding, F. Wu, G. Mailhot, D. Zhou, K. Hanna, Rapid catalytic oxidation of arsenite to arsenate in an iron (III)/sulfite system under visible light, Appl. Catal. B 186 (2016) 56–61.
[47] P. Neta, R.E. Huie, Free-radical chemistry of sulfite, Environ. Health Perspect. 64 (1985) 209.
[48] C. Brandt, R. Van Eldik, Transition metal-catalyzed oxidation of sulfur (IV) oxides. Atmospheric-relevant processes and mechanisms, Chem. Rev. 95 (1995) 119–190.
[49] A. Al-Anazi, W.H. Abdelraheem, C. Han, M.N. Nadagouda, L. Sygellou, M.K. Arfanis, P. Falaras, V.K. Sharma, D.D. Dionysiou, Cobalt ferrite nanoparticles with controlled composition-peroxymonosulfate mediated degradation of 2-phenylbenzimidazole-5-sulfonic acid, Appl. Catal. B 221 (2018) 266–279.
[50] W. Huang, M. Brigante, F. Wu, C. Mousty, K. Hanna, G. Mailhot, Assessment of the Fe (III)–EDDS complex in Fenton-like processes: from the radical formation to the degradation of bisphenol A, Environ. Sci. Technol. 47 (2013) 1952–1959.
[51] Y. Zhang, C. Liu, B. Xu, F. Qi, W. Chu, Degradation of benzotriazole by a novel

Fenton-like reaction with mesoporous Cu/MnO_2: Combination of adsorption and catalysis oxidation, Appl. Catal. B 199 (2016) 447–457.
[52] B. Jiang, Y. Liu, J. Zheng, M. Tan, Z. Wang, M. Wu, Synergetic transformations of multiple pollutants driven by Cr (VI)–sulfite reactions, Environ. Sci. Technol. 49 (2015) 12363–12371.
[53] C. Qi, X. Liu, Y. Li, C. Lin, J. Ma, X. Li, H. Zhang, Enhanced degradation of organic contaminants in water by peroxydisulfate coupled with bisulfite, J. Hazard. Mater. 328 (2017) 98–107.
[54] P. Neta, R.E. Huie, A.B. Ross, Rate constants for reactions of inorganic radicals in aqueous solution, J. Phys. Chem. Ref. Data 17 (1988) 1027–1284.
[55] Y. Ren, L. Lin, J. Ma, J. Yang, J. Feng, Z. Fan, Sulfate radicals induced from peroxymonosulfate by magnetic ferrospinel MFe_2O_4 (M= Co, Cu, Mn, and Zn) as heterogeneous catalysts in the water, Appl. Catal. B 165 (2015) 572–578.
[56] D. Zhou, L. Chen, C. Zhang, Y. Yu, L. Zhang, F. Wu, A novel photochemical system of ferrous sulfite complex: Kinetics and mechanisms of rapid decolorization of Acid Orange 7 in aqueous solutions, Water Res. 57 (2014) 87–95.
[57] J. Deng, Y. Shao, N. Gao, C. Tan, S. Zhou, X. Hu, $CoFe_2O_4$ magnetic nanoparticles as a highly active heterogeneous catalyst of oxone for the degradation of diclofenac in water, J. Hazard. Mater. 262 (2013) 836–844.
[58] L. Xu, W. Chu, N. Graham, A systematic study of the degradation of dimethyl phthalate using a high-frequency ultrasonic process, Ultrason. Sonochem. 20 (2013) 892–899.